Inorganica Chimica Acta, 18 (1976) 147–154

Single Crystal Properties of $[Cuen_3]SO_4$: Magnetic CD, Optical Intensity, and Convenient Method of Following Phase Transition

R. S. EVANS[1] and A. F. SCHREINER
Department of chemistry North Carolina State University Raleigh, North Carolina 27607, U.S.A.
Received August 6, 1975

A single crystal of (±)-$[Cuen_3]SO_4$ was studied by MCD and optically between 184° K and 274° K. The unique-axis spectra of this crystalline specimen and subsequent moment analysis show that there is (i) an apparent uniaxial ⇄ biaxial phase transition (ca. 180° K); (ii) C-term (C/D = 0.21 BM) behavior of the 16.0 kK band; (iii) vibronic optical intensity behavior of this band with $\nu \cong 200$ cm^{-1}; and (iv) the 8.5 kK band is a genuine electronic transition and not a vibrational overtone. It was also found that $[Cuen_3]^{2+}$ cannot be understood optically by assuming it to be of static D_3 symmetry; this infers that the effective symmetry for the electronic events is not D_3. A qualitative perturbation model is suggested which accounts for available electronic structural data of $[Cuen_3]^{2+}$ in relation to $[Cu(NO_2)_6]^{4-}$ and $[Cubipy_3]^{2+}$.

Introduction

Several studies of the d^9 (CuN_6) chromophore as $[Cuen_3]^{2+}$ are now available. The electronic ground state studies include the single-crystal X-ray structural analysis of $[Cuen_3]SO_4$ as the racemate, and it shows that Cu is at a D_3 site of this trigonal crystal.[2] ESR measurements demonstrate that at room temperature the g-value is isotropic (g = 2.110) in the (ab) plane (a = b here) but the electron distribution is somewhat anisotropic (g = 2.113 to 2.126) in the (ac) plane.[3] Below the phase transition, which is near 180° K (ref. 4 and this study), Bertini, Gatteschi and Scozzafava found three distinct g-values (2.053, 2.134, 2.159) from their ESR measurements.[4] Electronic excitations of $[Cuen_3]^{2+}$ salts were measured in solution by Bjerrum and Nielsen[5] and by Gordon and Birdwhistell[6], by reflectance spectroscopy by Hathaway, Bew, Billing, Dudley and Nicholls[7], and the single-crystal spectrum of undoped (±)-$[Cuen_3]SO_4$ was recently published by Bertini and Gatteschi.[8]

There is agreement by most investigators (*vide infra*) that the two low-intensity transitions observed (80° K) at 8.5 kK and 16.0 kK originate from *d–d* configuration change, $(t_{2g}^6 e_g^3) \rightarrow (t_{2g}^5 e_g^4)$, with octahedral state parentage $^2E_g \rightarrow {}^2T_{2g}$, but the suggestion has also been made[9] that the low energy excitation may be to a "tetragonal" component of ground state ^2E_g, and the high energy excitation is then to $^2T_{2g}$. Also, there remained a considerable number of other questions about the nature of these excited states, *e.g.*, their possible Jahn–Teller origin, trigonal or tetragonal field origin, and temperature dependence.

The higher energy excitation (16 kK) is the primary subject of this examination using variable temperature electronic optical and magnetic CD (MCD) techniques. Experience has shown that such examinations together can often lead to vitally complementing new information about electronic excited and ground states. It was of particular interest to explore whether or not MCD intensities would be affected by temperature changes, the role played by the spin–orbit coupling perturbation, and, perhaps, the Jahn–Teller effect.

Experimental

MCD measurements were made by placing the sample against a hot-finger ("hot" relative to dewar wall) dewar-insert sprung against the 77° K cylindrical bore, concentric with the 4.2° K bore, of a super-conducting magnet. The temperature of the sample was kept above the temperature of the phase-change (~180° K) by a resistance heater. Light from a 450 watt xenon lamp was monochromatized by a Spex 1400 (3/4 meter Czerny–Turner) double-monochromator, which is uniquely interfaced in a front-to-side manner with a JASCO ORD/UV/CD-5 (SS-20 modification) modified with appropriate additional focusing and collimating lenses and mirrors.

The crystal section employed in this study was taken from a long hexagonal specimen (*ca.* 2.5 mm × 2.5 mm × 4 mm). After cutting and polishing it, the section was found to be optically and spectroscopically correct for the MCD study. The final crystal was protected by a thin polymer layer. All MCD spectra were corrected for small depolarization.

The experimental density and crystal dimensions were used to compute the molar absorptivity. The elemental analysis of the crystal is as follows. $[Cuen_3]SO_4$, Calculated: C 21.20%, N 24.72%. Found: C 20.71%, N 24.08%.

Results and Discussion

The optical and MCD σ spectra were taken at several temperatures by passing light along the crystallographic c axis, which is also the (average) C_3 axis of the coordination species $[Cuen_3]^{2+}$ of the (±)-$[Cuen_3]SO_4$ crystal.[2] The crystal was not cooled lower than 184°K, since the nature of the phase transition[10] at *ca.* 180°K makes MCD (and natural CD) spectra of the cold phase meaningless. The basis for this statement is that we observed that the crystal became effectively very birefringent with cooling, suggesting a uniaxial (warm phase) ⇄ biaxial (cold phase) change, which was found to be reversible. This was detected here with great ease and convenience using modulated left- and right-circularly polarized light even in the absence of a magnetic field: the crystal has complete optical isotropy about the unique axis (warm phase), but on going through the phase change (*ca.* 180°K) the crystal develops immense CD activity just as expected of anisotropic biaxial crystals! Due to its convenience and sensitivity, this mode of detecting uniaxial ⇄ biaxial phase changes is expected to be generally useful and of great advantage over other techniques such as X-ray crystallography, since continuous variation of temperature and probe signal (CD or MCD activity) are so conveniently affected and monitored (Figure 1). In fact, the application of this procedure has recently led us to discover a previously unsuspected first-order phase transition[11] in $[Zn^{II}(OMPA)_3](BF_4)_2$, where OMPA is the uncharged ligand octamethylpyrophosphoramide, $[(H_3C)_2N]_2$

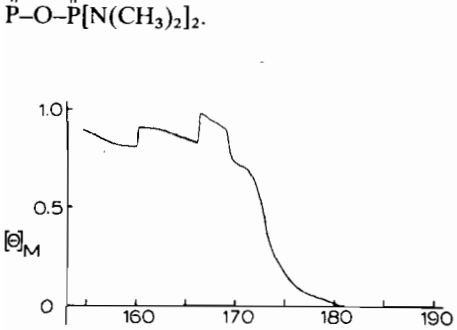

Figure 1. Phase transition of (±)-$[Cuen_3]SO_4$. Development of birefringe below 180°K of a uniaxial single-crystal specimen of (–)-$[Cuen_3]SO_4$. $[\Theta]_M$ is the natural molar ellipticity of the σ spectrum at 16 kK.

We now explore one possibility of interpreting the combined MCD and optical data, *i.e.*, on the basis of assuming that $[Cuen_3]^{2+}$ has static D_3 symmetry. This would be consistent with the polarizations[8] of the lower energy band at 8.5 kK (σ pol., or $^2E \rightarrow {}^2A_1$) and the higher energy band at 16.0 kK (σ and π pol., or $^2E \rightarrow {}^2E'$), and with the crystallographic result of (±)-$[Cuen_3]SO_4$. This interpretation of the polarization data leads to the conclusion that the two excited states derive from $^2T_{2g}(t_{2g}^5 e_g^4)$, and the order of components is $^2A_1 < {}^2E'$ (the ground state, ^2E_g, remains unsplit). The variation of MCD band intensities of the $^2E[^2E_g] \rightarrow {}^2E'[^2T_{2g}]$ (see Figures 2, 3) excitation observed between 274°K and 184°K is shown in Figure 3. This intensity increase with decreasing temperature is the expected Faraday C-term behavior of MCD spectra[12], *viz.*, $[\Theta(C)]_M = tH_z[f(\nu, \Delta, \nu_o) C(a \rightarrow j)/kT]$ where $t = -240N/hc$ and $C = (1/(2d_a))\Sigma <a|\mu_z|a> \cdot Im\{<a|m_x|j><j|m_y|a>$, all symbols having conventional meanings. The combined electronic absorption (*vide infra*) and MCD data lead to an experimental value of 0.21 BM for the ratio C/D of $^2E \rightarrow {}^2E'$ (Figure 4). For this band as a whole we find that at 274°K, for example, the Faraday B and C/kT values contribute 19% and 81% respectively to the overall observed intensity. The angular momentum of the ground state is therefore quite large. At this temperature C/kT and B have values of 7.31×10^{-5} and 1.67×10^{-5}, respectively, in units of δ^2 BM cm ($\delta \equiv$ Debye).

One may ask at this stage if it is possible to account for the observed C-term behavior (positive C/D) for the proposed transition $^2E[^2E_g] \rightarrow {}^2E'[^2T_{2g}]$ by neglecting spin–orbit coupling. In this approximation ($\zeta_{3d} = 0$) we derive $\frac{C}{D}(^2E \rightarrow {}^2E') = \frac{1}{2} <^2E^+|L_z|^2E^+>/d$ where d is a positive denominator, or $1 + <z>^2/(<x>^2 + <y>^2)$, and $|^2E^+>$ is a complex component of the *ground* state ^2E, or $|^2E^+> = (i/\sqrt{2})(|^2E_x> + i|^2E_y>)$. This integral $<^2E^+|L_z|^2E^+>$ vanishes in the ligand

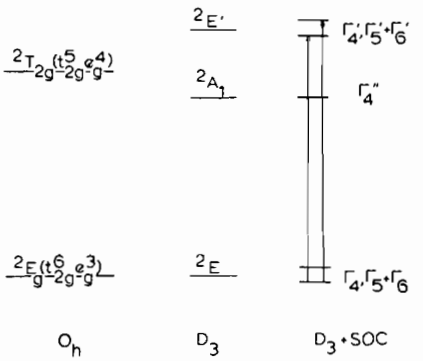

Figure 2. Energy level diagram of $[Cuen_3]^{2+}$ assuming static D_3 model (see Table I).

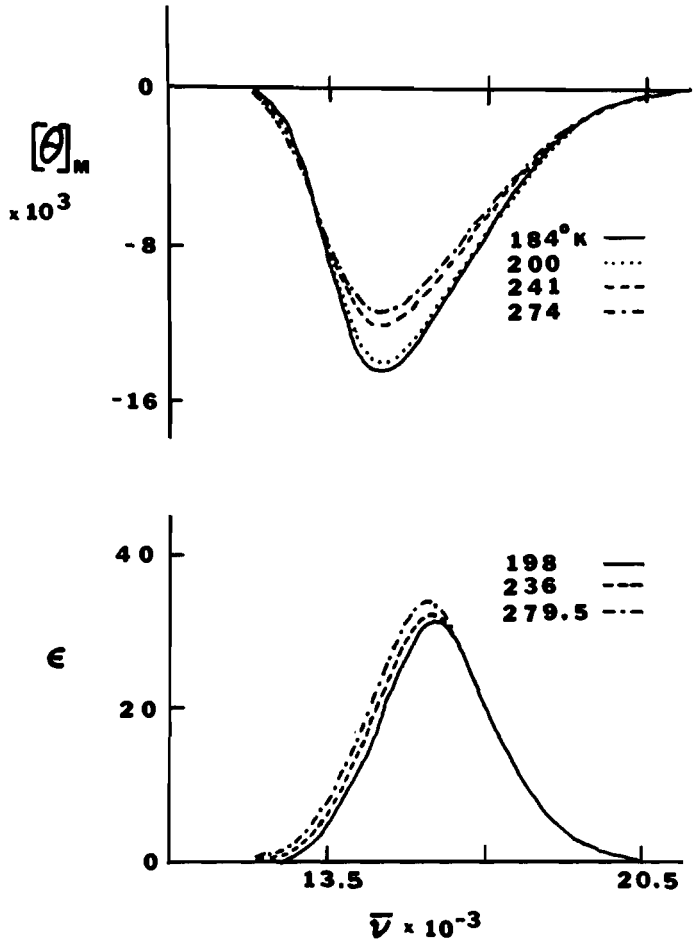

Figure 3. MCD and optical intensities at several temperatures of the σ band at 16 kK of a single crystal of (±)-$[Cuen_3]SO_4$.

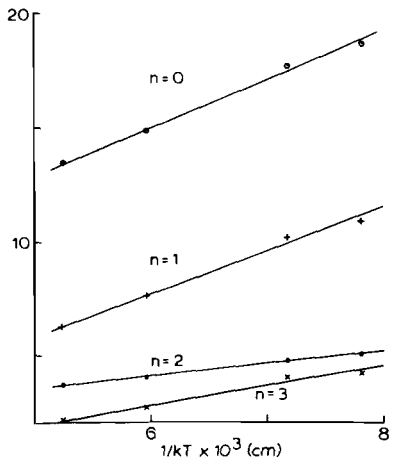

Figure 4. The variation of 0th, 1st, 2nd, and 3rd moments of the 16 kK MCD band of a single crystal of (±)-$[Cuen_3]SO_4$. Units are 10^{-4} BM/cm^{-1}, 10^{-1} BM, 10^{+3} BM/cm, and -10^6 BM/cm^2, respectively.

field model, since the function is defined as $|^2E^+> = 0.81650|d_1> - 0.57735\ |d_{-2}>$ for the "positron", and $|^2E^+>$ derives from ^2E_g. However, we investigated the contribution to $<L_z>$ which can be made by all atoms of the three ethylenediamine ligands and Cu. This calculation includes every kind of metal–ligand, ligand–ligand, and metal–metal (Cu, C, N, H) orbital angular momentum integral (1-, 2-, 3-center) possible, $<\chi_i|L_z|\chi_j>$. The full procedural details were previously described by Evans, Schreiner and Hauser,[13] the results being $<^2E^+|L_z|^2E^+> \cong 0.1$ BM and therefore C/D is equal to –0.05 BM. This sign can be reliably computed, as previously shown, but it is opposite the experimental sign. Thus, the exclusion of spin–orbit coupling from the D_3 model does not lead to an understanding of the experimental MCD data.

The second fact which calls for the consideration of spin–orbit coupling is that the MCD band minimum is about 1,100 cm^{-1} displaced from the optical maximum (Figure 3). This observation combined with the experi-

mental observation of C-term behavior is at least consistent with expecting the presence of two components, such as the pair of spin–orbit components of $^2E'$, under the apparent single optical band of the σ spectrum. Finally, the consequences of the very large one-electron spin–orbit coupling constant,[14] $\zeta_{3d} = 830$ cm^{-1} (free-ion), are expected to emerge as important molecular effects.

The data analysis via d^9 spin–orbit coupling in the D_3 ground and excited states, ^2E and $^2E'$, was carried out as follows. Spin–orbit coupling splits ^2E into $\Gamma_4(E_s)$, which has ordinary double-degeneracy, and $\Gamma_5(A_s)$ and $\Gamma_6(B_s)$, a Kramers' doublet. Similarly, $\Gamma_4'(E_s')$ and $\Gamma_5'(A_s')$ and $\Gamma_6'(B_s')$ derive from $^2E'$ (Figure 2). When the general C-parameter and dipole strength (D) expressions are expanded using these spin–orbit functions, we obtained for the σ polarization of our crystal experiment,

$$\Gamma_4 \rightarrow \Gamma_4' \quad C/D = (1/2)\langle \Gamma_4^+ | \mu_z | \Gamma_4^+ \rangle$$
$$\Gamma_4 \rightarrow \Gamma_{5,6} \quad C/D = -(1/2)\langle \Gamma_4^+ | \mu_z | \Gamma_4^+ \rangle$$
$$\Gamma_{5,6} \rightarrow \Gamma_4 \quad C/D = 0$$

All actual computations and derivations were carried out with ^2E and $^2E'$ and their spin–orbit components by considering these to arise from a single "positron", but all appropriate signs and phase were subsequently altered so as to make it a correct d^9 problem. The computed D_3 matrix elements of the energy matrix, **V**, are derived from applying the total perturbation Hamiltonian[15], V_t,

$$V_t = 10Dq[-\tfrac{1}{5}\sqrt{70}\, U_o^4 - 2(U_3^4 - U_{-3}^4)]$$
$$-v\,[\tfrac{1}{7}\sqrt{70}\, U_o^4 - \tfrac{4}{21}\sqrt{70}\, U_o^4 + \tfrac{2}{3}(U_3^4 - U_{-3}^4)]$$
$$+v'\,[\tfrac{4}{7}\sqrt{35}\, U_o^2 + \tfrac{4}{7}\sqrt{35}\, U_o^4 - \sqrt{2}(U_3^4 - U_{-3}^4)] + \zeta_{3d} V''$$

The last term is the spin–orbit coupling effect, U_n^m are unit tensors, and the basis is $|SLJM_J\rangle$ (Appendix).

Also, in order to ascertain a good choice of ligand field parameters consistent with this model it was desirable to confirm or counter the possible speculation[16] that the low energy band at 8.5 kK is a vibrational overtone of the (CuN_6) skeleton or ethylenediamine motions. For this purpose the optical mull spectrum of polycrystalline $[Znen_3]SO_4$ was measured and compared with $[Cuen_3]SO_4$ in the same spectral region (Figure 5). It is clearly evident that the 8.5 kK band is a genuine electronic excitation and is not to be associated with a vibrational overtone or combination band. To begin with, this band is much too wide to be a vibrational motion. However, we found vibrations on the red side of, and separated from, this optical band at 8.5 kK; the overall and fine-structure of the vibrations appear to be the same for the Zn^{2+} and

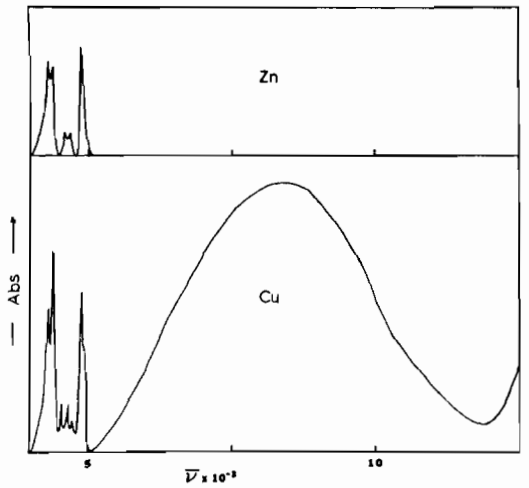

Figure 5. Ambient room temperature optical spectra of $[Cuen_3]SO_4$ and $[Znen_3]SO_4$.

Cu^{2+} complexes with energies close to overtones[17] of the SO_4^{2-} ion.

The computed energies using the above Hamiltonian and Dq = 1350 cm^{-1}, v = 7400 cm^{-1}, and $\zeta_{3d} = 830$ cm^{-1} (none of the conclusions below are affected by reducing ζ_{3d} by, for example, 40%) are given for this D_3 model in Table I. The ground state is split *ca.* 35 cm^{-1} with $\Gamma_4 < \Gamma_{5,6}$. Our Γ_4 ground state assignment ("M_J" = $\pm$ 1/2) appears confirmed by the agreement between our value of $g_z(2.16)$, $g_z = 2\langle \Gamma_4^+ | \mu_z | \Gamma_4^+ \rangle$, as computed with the ground state Γ_4 function, and the experimental value, 2.11, of the warm crystal phase. $^2E'$ is split about 816 cm^{-1}, close to the value of ζ_{3d}. The order of states of $^2E'$ is in general expected to be particularly pertinent to the MCD signs and intensity change with temperature, *viz.*, Γ_4' is predicted at lower energy and $\Gamma_{5,6}'$ at higher energy. This order is controlled by the sign of ζ_{3d}, about which there is no doubt. Furthermore, since Γ_4' is the lower energy component of E', the sign of the quantum mechanical C/D ratio for $\Gamma_4 \rightarrow \Gamma_4'$ must be the same as observed for the sign of the C term on

TABLE I. Spin–Orbit Energies of $[Cuen_3]SO_4$ (static D_3 model).

D_3	D_3+S.O.C.	Energies (kK)
^2E	Γ_4	0
	$\Gamma_{5,6}$	0.035
$^2A_1$	Γ_4	8.685
$^2E'$	Γ_4'	15.726
	$\Gamma_{5,6}'$	16.542

the red side of the MCD band (Figure 3). Since $\langle\Gamma_4^+|\mu_z|\Gamma_4^+\rangle = -1.08$ BM for the ground state, we have that C/D = –0.504 BM (*vide supra*). However, this negative C/D ratio (positive Θ) is opposite to what is found experimentally on the red side of $^2E'$! We also rule out the possibility that Boltzmann repopulation within the ground state, ^2E (see Figure 2), could account for the MCD intensity variation, on the basis that the 35 cm^{-1} separation of $\Gamma_{5,6}$ and Γ_4 will induce only about 2% intensity change between 270° K and 184° K, whereas we observe about a 10% intensity variation. This conclusion is valid even if the components were separated only 20 cm^{-1} (smaller ζ_{3d} than free-ion).

The composite of data leads us to conclude that the D_3 component of the ligand field of $[Cuen_3]^{2+}$ plays a very minor role in the optical spectroscopy of this complex ion.

The question of what possible role the Jahn–Teller effect plays in the distortion-favored ground state ^2E is highly interesting. A static Jahn–Teller effect is ruled out on three accounts. First, on considering stabilization from D_3 symmetry, $[Cuen_3]^{2+}$ would be allowed to distort only into a C_2 geometry. This distortion would produce two pairs of Kramers' doublets $\Gamma_{3,4}'$ deriving from the D_3 electronic excited state, $^2E'$ $[^2T_{2g}]$. The postulate of such a static electronic event being influential is unreasonable on the basis of MCD in view of the fact that $\Gamma_{3,4} \rightarrow \Gamma_{3,4}'$ transitions in C_2 will not create C-terms, which is in direct contradiction to our MCD measurement. Second, on the time scale of X-ray analysis there is also no evidence of a permanent distortion toward C_2. Instead, $[Cuen_3]^{2+}$ is at a crystal site of D_3 symmetry.[2] Third, the room temperature (warm phase) ESR spectrum[3] of $[Cuen_3]SO_4$ showed that g is isotropic in the (ab) plane, which is perpendicular to the C_3 axis of $[Cuen_3]^{2+}$, but g is somewhat anisotropic in the (ac) plane. This is consistent with the molecule-ion $[Cuen_3]^{2+}$ having D_3 and not C_2 symmetry in the room temperature environment. On the other hand, at liquid nitrogen temperature (*ca.* 80° K) three distinct g values ($g_1 = 2.053$, $g_2 = 2.134$ and $g_3 = 2.159$) were observed by Bertini, Gatteschi, and Scozzafava.[4] These values are for $[Cuen_3]SO_4$ in its cold crystal phase, here assigned to belong to a biaxial (<180° K) crystal system, so that three g values could at least in part be the result of the crystal environment. However, the possibility of "freezing out" Jahn–Teller distorted molecules of C_2 symmetry has also been suggested. This may be a contributing force for the phase change, *i.e.*, we have found recently[18] that a single crystal of (±)-$[Nien_3]SO_4$, which is unfavorable for Jahn–Teller distortion, stays uniaxial to *ca.* 15° K. We rule out this factor as being *dominant* in the $[Cuen_3]SO_4$ phase change, because our CD monitoring method indicates the completion of the phase change over a small temperature range (~10°), whereas the Jahn–Teller freeze-out is expected[19] to take place over a very large temperature range. We conclude that a $D_3 \rightarrow C_2$ static Jahn–Teller distortion does not account for the available data.

The second and third MCD moments of $^2E \rightarrow {}^2E'$ were also evaluated here in view of the recent suggestion by Robbins[20] that such a procedure may shed light on whether or not the dynamic Jahn–Teller effect is operative. The uncertain linearity or curvature of the values of the third moments *versus* 1/T leaves any conclusions that can be drawn from these plots in doubt (Figure 4).

We now turn to the optical spectrum for possibly other new insight (Figure 3). The axial optical spectrum of the 16.0 kK band is found to have a distinct temperature dependence, *i.e.*, it lost ~10% of its intensity when the temperature was lowered from 279.5° K to 198° K. When the behavior of dipole strength, D, *versus* temperature, T, is interpreted by means of the hyperbolic cotangent formula[21], $D = D_o \coth [\bar{\nu}/kT\ (cm^{-1})]$, an activating vibration of *ca.* 200 cm^{-1} can be concluded to be vibronically active. (CuN_6) skeletal modes are expected to have such energies. For example, the similar chromophore of $[Ni(NH_3)_6]^{2+}$ has a t_{1u} (NiN_6) skeletal bending mode[22] at ~220 cm^{-1}. This optical result leads one to favor a vibronic intensity gaining mechanism for this excitation. The remainder of results from zeroth and first moments[23] of the optical and MCD scans are given in Table II for this band, *i.e.*, the zeroth moments yield the dipole strength D and B+C/kT, and the first moment of the absorption spectrum yields ν_o for each temperature. It is evident from these data too that the D_3 portion of the total ligand field perturbation is far from sufficient for understanding the electronic excitations.

In addition to this optical vibronic behavior of $[Cuen_3]^{2+}$ and the MCD temperature dependence,

TABLE II. Optical and MCD Parameters for the 16 kK Band from Moment Analysis.

Optical T(° K)	$\bar{\nu}_o(cm^{-1})$	$D(\delta^2)^a$
198	15,910	5.78×10^{-2}
236	15,810	6.20×10^{-2}
279.5	15,710	6.65×10^{-2}
MCD		
T(° K)	B+C/kT[b]	(B+C/kT)/D[c]
184	10.64×10^{-5}	1.87×10^{-3}
200	10.39×10^{-5}	1.78×10^{-3}
241	9.29×10^{-5}	1.49×10^{-3}
274	8.98×10^{-5}	1.35×10^{-3}

[a] $\delta \equiv$ Debye. [b] δ^2 BM cm. [c] BM cm.

an explanatory model must also be able to account for the observation that the large separation of the excited states, perhaps of origin $^2T_{2g}(t_{2g}^5e_g^4)$, is similar for $[Cu(NO_2)_6]^{4-}$ (separation 9.6 kK)[24] and $[Cuen_3]^{2+}$ (separation 7.5 kK). This startling observation and the points raised above require one to abandon assigning the 7.5 kK splitting to a possible dominating, static trigonal electric field within $[Cuen_3]^{2+}$. The following unifying model (Figure 6) suggests itself and is consistent with available data.

The six octahedral N atoms of $[Cuen_3]^{2+}$ are considered to be dominant in affecting the *d*-electron localized behavior, *e.g.*, the *d–d* excitations under discussion here. For example, the very similar $[Nien_3]^{2+}$ behaves vibronically and has very low band intensities so that the effective optical symmetry is *ca.* O_h and not D_3. There are two stabilizing vibronic pathways available for distorting the octahedron, (CuN_6), *i.e.*, by means of e^v $(O\rightarrow D_4)$ or t_2^v $(O\rightarrow D_3)$ vibrations. We discount the latter distortion as a possibility here, since it does not remove the orbital degeneracy of the ground state ^2E $(t_2^6e^3)$ (also see below). The model is therefore based on a dynamic "tetragonal" (CuN_6) distortion dominating in the ground state. The model is also suggested because a normal tris-chelate may Jahn–Teller distort from ideal D_3 to C_2 symmetry via an $e^v(D_3)$ vibration.[25] Furthermore, the time-average of the dynamic tetragonal distortions in the three N–Cu–N directions of the chelate is also consistent with the crystal structure, since an average C_3 axis can still remain.

The suggested perturbation model weights several influences on ground and excited states as summarized in Figure 6. Here a dynamic, "tetragonal" Jahn–Teller effect on (CuN_6) removes the degeneracy of the unstable ground state ^2E_g via an e^v vibration. This is considered to be the largest perturbation, since the two observed excited states are separated by similar but large distances in $[Cuen_3]^{2+}$ (7.5 kK) as well as $[Cu(NO_2)_6]^{4-}$ (9.5 kK). The remaining and much less

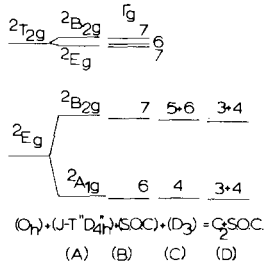

Figure 6. Dynamic Jahn–Teller perturbation model for $[Cuen_3]^{2+}$, (A)>(B)>(C). The label "D_{4h}", in (A) is italicized because "tetragonal" distortion of the six N atoms leads strictly to C_2 symmetry (final set of levels (D)) when account is taken of the presence of the $-CH_2CH_2-$ groups of en (level order of "D_{4h}" arbitrary).

influential perturbations of $[Cuen_3]^{2+}$ are spin–orbit coupling and molecular and crystalline trigonal fields (Figure 6). The model is consistent with all known data, *e.g.*, the temperature dependence of optical data (dominating perturbation is (A), Figure 6); the similar large excited state splitting of $[Cuen_3]^{2+}$ and $[Cu(NO_2)_6]^{4-}$ (latter lacks permanent trigonality); the time-average, crystallographic D_3 symmetry of $[Cuen_3]^{2+}$ in the warm phase ((CuN_6) skeletal distortion or (A) of Figure 6, plus $-CH_2-CH_2-$ of each en sum to a geometry of D_3); and the very small difference between ESR g values, g(ab) and g(ac) (similar result[26] for dynamic tetragonal Jahn–Teller distorted $[Cu(H_2O)_6]^{2+}$ in several types of crystals).

Also, ESR is the most sensitive ground state probe applicable to this problem, so that it ought to be most suited for sensing the nature of the relatively minor perturbations, *e.g.*, spin–orbit coupling and the D_3 field. The trigonal $\Gamma_4[^2E]$ ground state (Figures 2, 6) is "M_J" = $\pm$ 1/2 and has computationally (*vide supra*) the property of the ESR measurement.

There is still the question of whether the two excitations at 8.5 kK and 16.0 kK of $[Cuen_3]^{2+}$ are the result of very large splitting of the excited state, $^2T_{2g}$ (Figure 7 (A)), or the ground state, ^2E_g (Figure 7 (B)). The "tetragonal" splitting lifts the degeneracy (Figure 7 (B)) of ^2E_g but $^2T_{2g}(t_{2g}^5e_g^4)$ is expected to split relatively little. This model assigns the low-energy band to parentage ^2E_g and the high energy band to parentage $^2T_{2g}$. The band positions are given for $[Cu(NO_2)_6]^{4-}$, $[Cuen_3]^{2+}$ and $[Cuen_2]^{2+}$ in Figure 7 (B) along with the diagrams this model demands. The inferred order of Dq, $[Cu(NO_2)^6]^{4-}>[Cuen_3]^{2+}$, the separation of excited states, $[Cu(NO_2)_6]^{4-}>[Cuen_3]^{2+}$, and the tetragonal splittings of the ^1E_g ground state, $[Cuen_3]^{2+}<[Cuen_2]^{2+}$, are plausible and consistent with the model. It is assumed that the π-bonding of NO_2^- gives "N" of Cu–NO_2 a large effective mass, so that the splitting of ^2E_g is slightly smaller in [Cu

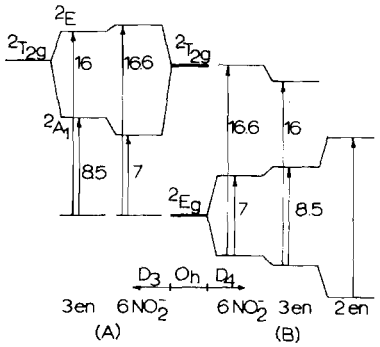

Figure 7. "Trigonally" (A) and "tetragonally" (B) dominant dynamic Jahn–Teller models of $[Cuen_3]^{2+}$. Each is strictly C_2 if $-CH_2CH_2-$ of en were a large perturbation optically.

$(NO_2)_6]^{4-}$ than in $[Cuen_3]^{2+}$. On the other hand, a "trigonal" dynamic Jahn–Teller distortion which takes (CuN_6) from an octahedron to a D_3 distortion is out of favor, *i.e.*, the distortion does not remove the degeneracy from this configurationally unstable ground configuration, and the D_3 diagram leads to 10 Dq being the same for $[Cuen_3]^{2+}$ and $[Cu(NO_2)_6]^{4-}$ as follows. Figure 7 (A) presents the data of $[Cuen_3]^{2+}$ and $[Cu(NO_2)_6]^{4-}$ as though it originated from a dominant trigonal distortion. In going from $[Cu(NO_2)_6]^{4-}$ to $[Cuen_3]^{2+}$ the positions of the high energy (^2E; 16.0 kK) and low energy (^2A; 8.5 kK) bands infer unreasonably that parent $^2T_{2g}$ of $[Cuen_3]^{2+}$ and $[Cu(NO_2)_6]^{4-}$ is above the ground state ^2E_g by a similar amount (Figure 7 (A)).

Finally, one may ask how much optical similarity there is between $[Cuen_3]^{2+}$ and $[Cubipy_3]^{2+}$. The variation of the optical intensities with temperature of the two excited states of the latter complex is very much smaller than what we find for $[Cuen_3]^{2+}$, and near room temperature the band intensities of $[Cubipy_3]^{2+}$ [27] are approximately twice as large as those of $[Cuen_3]^{2+}$. These comparative data are consistent with the view that a static, more dominant D_3 field is operative in $[Cubipy_3]^{2+}$, so that any potential "tetragonal" Jahn–Teller effect appears competitively quenched by presumably spin–orbit coupling. If $[Cuen_3]^{2+}$ data were attempted to be based on the same static D_3 model, Figure 8 can be used to try accounting for both sets of energy levels. Figure 8 (C) corresponds to the D_3 energy levels of $[Cubipy_3]^{2+}$, and the length of the arrows of Figure 8 (A) and (B) represent the transition energies of $[Cuen_3]^{2+}$ drawn so that either the low energy (Figure 8 (A)) or high energy (Figure 8 (B)) band fits the diagram. Clearly, $[Cuen_3]^{2+}$ does not fit the D_3 diagram. Additional information is expected to evolve from our detailed MCD study of crystals containing $[Cubipy_3]^{2+}$ and the spin–orbit–vibronic analysis of $[Cuen_3]^{2+}$.

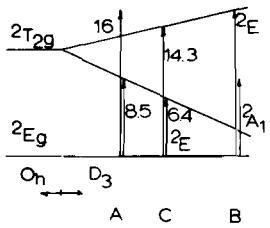

Figure 8. Attempt to fit optical data of $[Cuen_3]^{2+}$ to trigonal model of $[Cubipy_3]^{2+}$ (B) (see text).

Appendix

The d^1 crystal field perturbation matrices over the free–ion basis, $|SLJM_J>$, of $^2D_{5/2}$ and $^2D_{3/2}$ first required the derivation of these functions. Therefore, Clebsch–Gordon coefficients were obtained so as to be able to express functions of $|SLJM_J>$ as linear combinations of $|SLM_LM_S>$ functions, $|(2S+1)LJM_J> = \Sigma\ C(M_L,M_S;J,M_J)|(2S+1)LM_LM_S>$. The necessary transformation matrix, T, of $\mathbf{J} = \mathsf{T}\,\mathbf{L}$ is the result, where $\mathbf{J}$ is a column vector of $|JM_J>$ and $\mathbf{L}$ is a column vector of $|M_LM_S>$:

$$
\begin{bmatrix} 5/2 & 5/2 \\ 5/2 & 3/2 \\ 5/2 & 1/2 \\ 5/2 & -1/2 \\ 5/2 & -3/2 \\ 5/2 & -5/2 \\ 3/2 & 3/2 \\ 3/2 & 1/2 \\ 3/2 & -1/2 \\ 3/2 & -3/2 \end{bmatrix} =
\begin{bmatrix}
1 & 0 & 0 & 0 & 0 & 0 & 0 & 0 & 0 & 0 \\
0 & \sqrt{\frac{4}{5}} & 0 & 0 & 0 & \sqrt{\frac{1}{5}} & 0 & 0 & 0 & 0 \\
0 & 0 & \sqrt{\frac{3}{5}} & 0 & 0 & 0 & \sqrt{\frac{2}{5}} & 0 & 0 & 0 \\
0 & 0 & 0 & \sqrt{\frac{2}{5}} & 0 & 0 & 0 & \sqrt{\frac{3}{5}} & 0 & 0 \\
0 & 0 & 0 & 0 & \sqrt{\frac{1}{5}} & 0 & 0 & 0 & \sqrt{\frac{4}{5}} & 0 \\
0 & 0 & 0 & 0 & 0 & 0 & 0 & 0 & 0 & 1 \\
0 & -\sqrt{\frac{1}{5}} & 0 & 0 & 0 & \sqrt{\frac{4}{5}} & 0 & 0 & 0 & 0 \\
0 & 0 & -\sqrt{\frac{2}{5}} & 0 & 0 & 0 & \sqrt{\frac{3}{5}} & 0 & 0 & 0 \\
0 & 0 & 0 & -\sqrt{\frac{3}{5}} & 0 & 0 & 0 & \sqrt{\frac{2}{5}} & 0 & 0 \\
0 & 0 & 0 & 0 & -\sqrt{\frac{4}{5}} & 0 & 0 & 0 & \sqrt{\frac{1}{5}} & 0
\end{bmatrix}
\begin{bmatrix} 2 & 1/2 \\ 1 & 1/2 \\ 0 & 1/2 \\ -1 & 1/2 \\ -2 & 1/2 \\ 2 & -1/2 \\ 1 & -1/2 \\ 0 & -1/2 \\ -1 & -1/2 \\ -2 & -1/2 \end{bmatrix}
$$

The application of these functions to the matrix of the $Y_4^3-Y_4^{-3}$ operator of d^1, which is, in the $|M_LM_S>$ basis,

M_L	2	1	0	−1	−2
2				−1/14	
1					1/14
0					
−1	−1/14				
−2		1/14			

in units of $(35/\pi)^{1/2}$, yielded this d^1 operator in the $|JM_J>$ basis. The remaining perturbation matrices, Y_2° and Y_4°, were treated similarly. Inclusion of the spin–orbit compling matrix,

	$^2D_{5/2}$	$^2D_{3/2}$
$^2D_{5/2}$	1	0
$^2D_{3/2}$	0	−3/2

(in reduced form; units of ζ_{3d}) allowed the calculation of eigenvalues (Table I) and eigenvectors of $[Cuen_3]SO_4$.

Acknowledgements

Acknowledgement is made to the donors of The Petroleum Research Fund, administered by the American Chemical Society; the Research Corporation; and to the School of Physical and Mathematical Sciences of North Carolina State University for support of this research. We thank I. Bertini and D. Gatteschi of Florence for a crystal specimen and for drawing our attention to the optical data of $[Cu(NO_2)_6]^{4-}$.

References

1 American Chemical Society Petroleum Research Fund Fellow.
2 D.L. Cullen and E.C. Lingafelter, *Inorg. Chem., 9,* 1858 (1970).
3 R. Rajan and T.R. Reddy, *J. Chem. Phys., 39,* 1140 (1963).
4 I. Bertini, D. Gatteschi and A. Scozzafava, *Inorg. Chim. Acta, 11,* 217 (1974).
5 J. Bjerrum and E.J. Nielsen, *Acta Chem. Scand., 2,* 307 (1948).
6 G. Gordon and R.K. Birdwhistell, *J. Am. Chem. Soc., 81,* 3567 (1959).
7 B.J. Hathaway, M.J. Bew, D.E. Billing, R.J. Dudley and P. Nicholls, *J. Chem. Soc. (A),* 2312 (1969).
8 I. Bertini and D. Gatteschi, *Inorg. Nucl. Chem. Letters, 8,* 207 (1972).
9 C.K. Jorgensen, *Acta. Chem. Scand., 9,* 1362 (1955).
10 Ref. 4 and observation at this laboratory.
11 Observation at this laboratory.
12 A.D. Buckingham and P.J. Stephens, *Ann. Rev. Phys. Chem., 17,* 399 (1966).
13 R.S. Evans, A.F. Schreiner and P.J. Hauser, *Inorg. Chem., 13,* 2185 (1974).
14 B.N. Figgis, "Introduction to Ligand Fields", Interscience, New York, N.Y. (1966).
15 R.M. MacFarlane, *J. Chem. Phys., 39,* 3118 (1963).
16 R.A. Palmer, private communication.
17 K. Nakamoto, "Infrared Spectra of Inorganic and Coordination Compounds," Wiley, New York (1963).
18 D.J. Hamm and A.F. Schreiner, *Chem. Phys. Letters, 29,* 140 (1975).
19 B. Bleaney, K.D. Bowers and R.S. Trenam, *Proc. Roy. Soc. (London), 228A,* 157 (1955).
20 D.J. Robbins, *Theoret. Chim. Acta, 33,* 51 (1974).
21 C.J. Ballhausen, "Introduction to Ligand Field Theory," McGraw-Hill, New York, N.Y. (1962).
22 D.M. Adams, "Metal–Ligand and Related Vibrations: A Critical Survey of the Infrared and Raman Spectra of Metallic and Organometallic Compounds," St. Martin's, Press, New York, N.Y. (1968).
23 C.H. Henry, S.E. Schnatterly and C.P. Slichter in "Physics of Color Centers," W.B. Fowler Ed., Academic Press, New York, N.Y. (1968).
24 B.J. Hathaway and D.E. Billing, *Coordin. Chem. Rev., 5,* 143 (1970).
25 R. Englman, "The Jahn-Teller Effect in Molecules and Crystals," Wiley–Interscience, New York, N.Y. (1972).
26 A. Abragam and M.H.L. Pryce, *Proc. Phys. Soc. (London), 63A,* 409 (1950); B. Bleaney and K.D. Bowers, *ibid., 65A,* 667 (1952); and ref. 19.
27 R.A. Palmer and T.S. Piper, *Inorg. Chem., 5,* 864 (1966).